

# Thermoregulating gypsums by using nanoencapsulated phase change material slurry

Daniel López Pedrajas<sup>1</sup>, Ana M. Borreguero Simón<sup>1</sup>, I. Garrido Sáenz<sup>2</sup>, F. Javier Ramos<sup>1,3</sup>, Juan F. Rodríguez Romero<sup>1</sup>, Manuel Carmona Franco<sup>1</sup>

<sup>1</sup>University of Castilla-La Mancha, Department of Chemical Engineering, Institute of Chemical and Environmental Technology. Ciudad Real, Spain.

<sup>2</sup>University of Castilla-La Mancha, Department of Applied Mechanics and Engineering Projects, School of Architecture. Toledo, Spain.

<sup>3</sup>University of Castilla-La Mancha, Department of Vegetal Production and Agricultural Technology, Higher Technical School of Agricultural and Forestry Engineering, Albacete, Spain

\*Corresponding author: e-mail: Manuel.CFranco@uclm.es

**Keywords:** PCM, nanoencapsulated PCM slurry, nanocapsule, gypsum, thermal properties, mechanical properties, thermal energy storage

## Abstract

Thermoregulating composites were produced by using a thermoregulating slurry (NPCS) containing nanoencapsulated phase change material (NPCM) from poly(styrene-co-divinylbenzene) as shell and the commercial paraffin Rubitherm<sup>®</sup>RT27 as core material. These composites were synthesized by using the constitutive water of the slurry as setting water and changing the NPCM/Hemihydrate (NPCM/Hem) mass ratio within 0.0-0.41. It was found that nanoparticles were uniformly dispersed into the gypsum, and the gypsum crystal morphology was tuned by the addition of the slurry. Attending to the thermal properties, these materials can work either as insulating or thermal energy storage materials, decreasing the thermal conductivity up to ~50 %, whereas the thermal energy storage (TES) capacity is enlarged in a ~140 %, respect to the pure gypsum, when the maximum NPCM/Hem mass ratio was used. This gypsum composite showed a latent heat of 30.2 J g<sup>-1</sup> and a heat capacity of equivalent 3.5 J g<sup>-1</sup>K<sup>-1</sup>. Composites from a NPCM/Hem mass ratio up to 0.15 satisfied European mechanical standard EN 13279-1 for gypsum binders and gypsum plasters and all of them, presented a bulk density higher than 0.60 g cm<sup>-3</sup>. The addition of a 41 % in mass of nanocapsules saved 13.5 kWh m<sup>-3</sup> and, reduced CO<sub>2</sub> emission up to 3.4 kg of CO<sub>2</sub> per operating cycle. The use of this new material would lead to significant energy and economic savings, as well as a considerable reduction in the emission of polluting gasses into the atmosphere.

## Introduction

The world energy consumption is expected to rise nearly 50 % by 2050 [1]. This quick and high growing energy demand can generate a depletion of resources, supply difficulties and destructive environmental impact. 50 % of the EU's energy consumption is used for heating and cooling, from which 80 % is consumed in buildings [2,3]. Consequently, the 2015 Paris Agreement established a series of objectives to renovate the housing stock, prioritizing energy efficiency by improving the thermal insulation or applying new building designs, promoting the development and use of sustainable energy resources [3,4]. Buildings present a large surface exposed to the sun light, being possible to use this renewable energy as an alternative source to satisfy their thermal energy demands [5]. However, this energy has a low density and is intermittent, which hinders its collection and storing.

The sensible heat of materials for the sun energy storage has been widely used in buildings. However, in recent years, the usage of the latent heat has gained and is now one the most studied alternatives because of the high thermal capacity per mass unit and the absence of temperature change during the phase transition make this alternative very attractive for thermal energy storage (TES) [6]. Phase change materials (PCMs) are substances that are able to absorb and store large amounts of thermal energy in the form of latent heat. The mechanism of PCMs for energy storage relies on the increased energy need of some materials to undergo phase transition. A PCM, absorbs or releases energy by taking advantage of its latent heat when temperature undergoes or overpasses its melting point [7].

PCMs can be applied in two types of TES systems, namely passive or active energy storage systems. In passive energy storage, the PCM is incorporated into building materials. Active energy storage strategies cover heating, ventilation and air conditioning (HVAC) systems, where a new kind of fluid appears, the named Phase Change Slurry (PCS). The PCS is a fluid composed of a continuous liquid phase, such as water, and a dispersed solid one (PCM) which is stable and behaves as a fluid, which permits easy transportation of and pumping into active energy storage systems [8,9].

The passive systems have been implemented and studied since 1980 [10] by incorporating the PCM in the walls, shutters, ceilings and floors, for which gypsums, concrete and polyurethane foams are frequently used [4,11,12].

However, some authors have reported undesirable interactions of the PCMs and the building material or their leakage when they are incorporated directly [13,14]. These problems can be solved by encapsulating the PCMs before mixing with the building material. One of the first and better studied polymer shells for PCM microencapsulation is polystyrene [15–18]. However, these microcapsules presented low mechanical resistance [19], resulting in a bad choice for long-lasting applications such as the enhancement of building thermal comfort. To overcome this drawback, polystyrene has been copolymerized with methyl-methacrylate [20–22] and with divinyl-benzene [23], resulting in similar thermal energy storage capacities. Polymethylmethacrylate [24–26] and melamine–formaldehyde [27–30] polymer shells have been also widely investigated for PCMs microencapsulation. However, their application in buildings seems to reduce the mechanical properties greater than those made with poly(styrene-co-divinylbenzene) shells [31,32]. Besides, the methyl-methacrylate derived polymers tend to present related swelling problems. On the other hand, low density polyethylene and ethyl vinyl acetate copolymers [19] or polymers derived from chitosan (CS) and carboxymethyl cellulose [33] have been also employed but they are produced by methods incompatible with the production of a stable slurry. Thus, a PCS from poly(styrene-co-divinylbenzene) copolymer was selected as the most suitable thermal liquid for manufacturing gypsum composites.

On the other hand, although there is extensive research on the use of microcapsules (1 – 1000  $\mu\text{m}$ ) (MPCM) in TES [11,16,34], the current trend is the submicron- (0.1–1  $\mu\text{m}$ ) or nanoencapsulation ( $\leq 100 \text{ nm}$ ) of the PCM [35,36], since they presented better long-term stability, higher heat transfer area and better structural stability [37,38]. Borreguero, A. M. *et al.* [12] manufactured smart gypsum composites by adding different kinds of MPCMs in order to develop building materials with high TES capacity. The incorporated MPCMs had an average particle size between 3 - 117  $\mu\text{m}$ . They achieved up to 15 wt% of MPCMs with respect to the hemihydrate (Hem), obtaining a TES capacity of  $10.57 \text{ kW m}^{-1}\text{K}^{-1}$  and a decrease in thermal conductivity, with a minimum value of  $0.20 \text{ W m}^{-1}\text{K}^{-1}$ . However, they observed a non-homogeneous distribution of MPCMs throughout the gypsum matrix, as well as a large amount of particle agglomerations, and this effect worsened with increasing capsule size and the amount of MPCMs in the composites. There are further investigation of MPCMs addition in

gypsums [39–41] with these same problems, which may result in areas with worse thermal properties than others, as well as a worsening of mechanical properties.

On the other hand, Mohammadi, B. *et al.* [20] incorporated nanocapsules of butyl palmitate as core and polystyrene-co-methyl methacrylate as shell in a gypsum wall. They demonstrated that compared with the unmodified gypsum, the gypsum wall containing NPCM took longer time to get to the thermal equilibrium, 600 and 8400 s, respectively. Maleki, B. *et al.* [21] synthesized submicrocapsules (SPCMs) from polymethylmethacrylate modified with CuO nanoparticles containing *n*-dodecanol as phase change material. They manufactured gypsum-SPCM composites at reduced-scale considering a small room with PCM and another one without it. The results indicated that the PCM system exhibited narrow indoor air temperature fluctuations and maintained the indoor thermal comfort for most of the year. They achieved an increase in heat capacity and a decrease in thermal conductivity of ~50 and ~47 %, respectively, for 50 % by mass of SPCMs with respect to the hemihydrate. However, these previous investigations did not study the NPCM distribution in the composite material and their influence on the physical and mechanical properties of the new building material. Smart gypsum composite boards up to 30 wt% *n*-octadecane NPCMs were fabricated by Khadiran, T. *et al.* [22]. They observed a reduction in the density, both bulk and real, of the building materials with the increase of the NPCMs load, as well as an increase in porosity. They detected, as well, a non-homogenous dispersion of the NPCMs in the gypsum matrix by FESEM. Nevertheless, the smart gypsum had good thermal properties, obtaining a reduction in indoor temperature of 4.6 K respect to the gypsum without NPCMs. As in the previous mentioned work, the mechanical properties of the smart gypsum were not studied.

In a previous work, it was found that the particle size of the capsules and the agglomeration played an important role in the final composites properties [12]. To the best of our knowledge, the use of a concentrated slurry containing PCM nanocapsules with particles size lower than 100 nm to hydrate the hemihydrate, allowing the development of gypsum composites, presenting homogeneous filler distribution, large thermal energy accumulation and low subcooling, without losing their insulating capacities has not been reported yet. Some articles described the production of gypsum boards containing PCMs but the fillers used do not satisfy the European Commission and ISO/TS 80004–1 classification as nanomaterials, where most of the half of nanoparticles

(in number) must be below 100 nm and also those gypsum blocks did not keep the thermal conductivity of the original gypsum.

In this research, a NPCS has been synthesized following our patent [42], containing NPCMs from poly(styrene-divinylbenzene) with paraffin wax Rubitherm®RT27 as PCM. Hence, thermally enhanced gypsums have been produced, employing such NPCS as additive. It was possible to reach a filler content up to 41 % of NPCM with respect to the gypsum hemihydrate (Hem). The physical, morphological, thermal and mechanical properties of the developed composites have been studied.

## Materials and methods

### Materials

Black gypsum, supplied by BigMat S.A. and milli-Q water with a conductivity value lower than  $5 \mu\text{S cm}^{-1}$  were used for fabricating the gypsum blocks composites. The nanoencapsulated PCM slurry (NPCS) was synthesized by the chemical engineering department of the University of Castilla-La Mancha according to the patent number ES2804063 [42]. The characteristics of this NPCS, the NPCM concentration (in mass) in the NPCS ([NPCM]) measured by gravimetry, the zeta potential ( $\zeta$ ) by Doppler laser microelectrophoresis technique, the particle size in volume and number ( $dv_{0.5}$  and  $dn_{0.5}$ , respectively) by Dynamic Light Scattering (DLS) and the latent heat of the NPCM ( $\Delta H_{\text{NPCM}}$ ) by Differential Scanning Calorimetry (DSC) are listed in the Table 1.

**Table 1.** Characteristics of the NPCS added to the gypsums.

| [NPCM] (%) | $\zeta$ (mV) | $dv_{0.5}/dn_{0.5}$ (nm) | $\Delta H_{\text{NPCM}}$ (J g <sup>-1</sup> ) | Melting point (K) |
|------------|--------------|--------------------------|---|-------------------|
| 38.5       | - 53.5       | 117.7/78.7               | 103.3   | 298.5             |

### Gypsum composites fabrication

Gypsum blocks were synthesized by first weighing the known mass of nanoencapsulated PCM slurry (NPCS) for obtaining the desired mass ratio of PCM-based nanocapsules regarding to the hemihydrate (NPCM/Hem). Then, when an extra amount of water was required (in addition to the water from NPCS), it was added to the mixer container to keep a constant water/Hem mass ratio at 0.6. After that, the required mass of Hem was included together with the mixture NPCS-water using a mixer that satisfies the European regulation UNE-EN 196-1 [43]. The mixing process is carried out at slow speed for 1.5 min. Finally, the mixture was poured into a mold of 40×40×160 mm for the

mechanical test, to a mold of 30×60×100 mm for the thermal analysis and to a mold of 20×110×110 mm for the studying the thermal conductivity in lambdometer. The composites will be named as C-NPCM/Hem<sub>x</sub>, where “x” is the PCM nanocapsule content in mass regarding hemihydrate (NPCM/Hem mass ratio). The recipes used for the manufactured C-NPCM/Hem are shown in Table 2.

**Table 2.** Amount of Hem, NPCS and water in mass for the manufactured composites.

| <b>Composites</b>        | <b>Hem (%)</b> | <b>NPCS (%)</b> | <b>Additional water (%)</b> |
|--------------------------|----------------|-----------------|-----------------------------|
| C-PS/Hem <sub>0</sub>    | 62.5           | 0.0             | 37.5                        |
| C-PS/Hem <sub>0.1</sub>  | 58.4           | 15.2            | 26.5                        |
| C-PS/Hem <sub>0.15</sub> | 56.5           | 22.0            | 21.5                        |
| C-PS/Hem <sub>0.2</sub>  | 54.8           | 28.4            | 16.8                        |
| C-PS/Hem <sub>0.3</sub>  | 51.6           | 40.2            | 8.3                         |
| C-PS/Hem <sub>0.42</sub> | 48.5           | 51.5            | 0.0                         |

## **Characterization**

### *Fourier Transform Infrared (FT-IR) spectroscopy*

Fourier Transform Infrared (FT-IR) spectroscopy analysis was carried out on a Spectrum Two spectrometer (Perkin Elmer, Inc) equipped with a Universal Attenuated Total Reflectance (UATR) accessory. Three samples in different positions of the same specimen were carried out, and an average value has been taken as a result. All infrared spectra were collected using 16 scans and 16 cm<sup>-1</sup> resolution in the wavelength range of 4000 to 500 cm<sup>-1</sup>.

### *Scanning Electron Microscopy (SEM) analysis*

Manufactured gypsum composites were depicted by means of Scanning Electron Microscopy (SEM) by using a Quanta 250 (FEI Company) with a tungsten filament operating at a working potential of 15 to 20 kV. The Backscattered Electron Detector (BSED) was applied for imaging.

### *X-Ray Diffraction (XRD) analysis*

The crystallography of the obtained materials was analyzed by using an X-ray diffractometer (Philips) model X, Pert MPD. The equipment has a radiation CuKα1, automatic divergence slit, graphite monochromator and xenon gas sealed detector.

### *Thermogravimetric Analyses (TGA) of gypsum composites*

The thermal stability of the synthesized composites was analyzed by Thermogravimetric analysis (TGA) using a SDT Q600 Simultaneous DSC-TGA (TA Instruments). Three different samples in different positions from the same gypsum composite specimen were carried out, in order to study the homogeneity of the composites. Those samples were taken with a spatula from the mechanical specimen gypsums blocks at 0, 200 and 400 mm. The total sample mass was around 2 g. Temperature was tuned from room temperature to 973 K, under a nitrogen atmosphere and using a heating rate of 10 K min<sup>-1</sup>.

#### *Density and porosity*

The bulk density of the gypsum block ( $\rho_{bulk}$ ) was determined by weighing and sizing the specimens. The real density ( $\rho_{real}$ ) was determined by helium pycnometry (Micromeritics AccuPy II 1340). The porosity of the gypsum composites ( $\varepsilon$ ) were estimated with the Eq. 1 from the  $\rho_{bulk}$ ,  $\rho_{real}$  and assuming that the gypsum pores are filled of air which remains trapped once the gypsum has solidified. The air density ( $\rho_{air}$ ) was assumed to be 0.001 g cm<sup>-3</sup>, which corresponds to the  $\rho_{air}$  at normal conditions.

$$\varepsilon = \frac{\rho_{real} - \rho_{bulk}}{\rho_{real} - \rho_{air}} \quad [1]$$

#### *Procedure and experimental equipment thermal behavior tests of the composite gypsum blocks*

The thermal behavior of gypsum composites with NPCS additive with NPCS has been analyzed using a homemade apparatus, where the different temperature profiles of the specimens are measure over time when they are subjected to hot or cold on one of its faces and always starting from a steady state to a new one as temperature function. The apparatus consisted of an aluminum box having a thickness of 1 mm through which a liquid coming from a thermostatic bath was circulated by a peristaltic pump. The temperature of the aluminum cell was controlled by the temperature of this liquid. The specimen chamber in the apparatus was 30×60×100 mm, the same dimensions of the tested specimen. Each gypsum block was place on the upper surface of the cell and further insulated with foams boards of 4 cm in thickness. This assemblage is put inside of a thermostatic chamber which maintains the internal temperature at 298 K. A more exhaustive description of the equipment and of its performance for the thermal characterization of materials were described and proved in previous works [11,44–46].

Tests were carried out applying a thermostatic bath set-point steps change from 291 to  $318 \pm 0.1$  K and from  $318$  to  $291 \pm 0.1$  K. Six thermocouples of K-type were used to measure temperatures: two were put in the external specimen surface ( $T_{up}$ ), other two were placed at the middle of the specimen ( $T_{middle}$ ) and the last ones in the cell ( $T_{down}$ ). The liquid flow was a flow of  $9 \text{ L h}^{-1}$  to ensure the absence of thermal profile in liquid direction. Six heat flow sensors gSKIN®-XI and gSKIN®-XP were placed on each face of the specimen in order to monitor online the inlet and outlet heat fluxes. Fig. 1 shows the distribution of the thermocouples and heat flow sensors in the specimen studied. The signals of the thermocouples and heat flow sensors were registered continuously using the NOKEVAL program and recorded by means of a computer. Using these signals, it is possible to quantify the, the TES ( $\text{kWh m}^{-3}$ ) capacity per cubic meter (Eq. 2) of the gypsum composite:

$$\text{TES capacity} = \frac{q_{acc}}{m_{sample}} \times \frac{\rho_{bulk}}{3.6 \times 10^6} \quad [2]$$

Where  $q_{acc}$  is the amount of accumulated heat in the sample during the experiment (J),  $m_{sample}$  is the specimen mass (kg).

The thermal characterizations were performed three times.

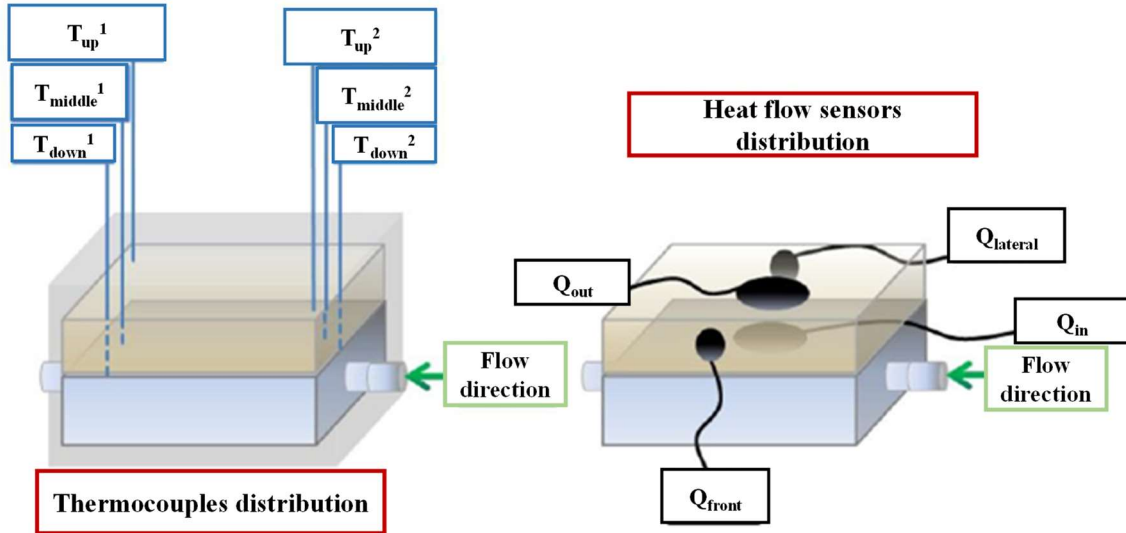


**Fig. 1.** Scheme of heat flow sensors and thermocouples in the homemade apparatus for studying the thermal behavior of gypsum composites.



### *Differential Scanning Calorimetry (DSC)*

The DSC model 214 Polyma from Netzsch (equipped with a cooling system and nitrogen at 40 mL min<sup>-1</sup> as the purge gas) was used to measure the  $c_p$  of the gypsums block composites employing Proteus Analysis software to analyze data. In particular, the software extension “Ratio Methat” allowed to obtain the  $c_p$  value of the material. DSC was carried out in three samples taken at different positions (0, 20 and 40 mm) of the same gypsums composite specimen to demonstrate the homogenous distribution of the nanocapsules contained in it. Sapphire was used as calibration or reference material before measuring the sample in order to obtain the real heat capacity of composites at each temperature (not only the differential heat flux regarding air), using the abovementioned proteus Analysis software extension to analyze data. So, in order to carry out the measure of the sample  $c_p$ , the following methodology was followed:

1. Blank measurement (empty crucible).
2. Sapphire measurement as standard (reference material).
3. Sample measurement of the gypsum composite to evaluate the material  $c_p$ .

For the three steps, the same temperature ramp was used (253 to 323 K, up and down, at 3 K min<sup>-1</sup>). The latent heat capacities were determined by integrating the  $c_p$  curve regarding to the baseline.

For thermal cycling (heating /cooling) of the thermoregulating gypsum with the maximum load in NPCM (41 %, in mass), such temperature cycle was performed between 263 and 313 K, at a heating/cooling rate of 3 K min<sup>-1</sup> to ensure the applicability of the gypsum composite in realistic operating cycles.

### *Lambda meter*

A lambda meter model HFM 446 Lambda medium (NETZSCH) was used, in order to quantify the thermal conductivity. In that way, thermal conductivity of different specimens with dimensions of 110×110×20 mm were measured at 281, 289, 297, 301, 305, 313 and 318 K with a temperature gradient of 20 K between upper and bottom plates.

### *Mechanical tests*

The mechanical properties of the gypsum composites were studied by using a Servohydraulic Test System (MTS Landmark). The flexion and compressive strengths were calculated according to standard UNE-EN 13279-2 [47]. The flexion test was done using specimens samples of 40×40×160 mm applying a load rate of 50 N s<sup>-1</sup> until fracture. The compression test was done using the broken flexion test specimens. A load rate of 1 N mm<sup>-2</sup>s<sup>-1</sup> was applied over 40×40 mm surface load application until fracture. From these results, the Young's modulus (E) is determined as the slope value of the initial part of the compression curves. The mechanical tests were performed three times at room temperature (293 K), three times at PCM melting point (308 K) and three times when the whole PCM is melted (318 K).

## Results and discussion

### Fourier transform infrared spectroscopy

To confirm the presence of the NPCM in the gypsum blocks, FT-IR spectroscopy analyses were performed in three different positions of the same specimens for each NPCM/Hem mass ratio. As an example, the media of the FT-IR spectra of the C-NPCM/Hem<sub>0</sub>, C-NPCM/Hem<sub>0.2</sub> and C-NPCM/Hem<sub>0.41</sub> and the FT-IR spectra of the pure NPCM are shown in Fig. 2. In the FT-IR spectra of the NPCM appear the three characteristic absorption bands for paraffin wax: rocking vibration of -CH<sub>2</sub> at 721 cm<sup>-1</sup>; deformation vibration of -CH<sub>2</sub> and -CH<sub>3</sub> at 1466 cm<sup>-1</sup>; and three intensive peaks between 3000 - 2840 cm<sup>-1</sup>, which correspond to alkyl stretching vibrations of -CH<sub>2</sub> and -CH<sub>3</sub> [48,49]. This spectrum presents also absorption bands at 3020, 750 and 695 cm<sup>-1</sup>, attributed to aromatic C-H stretching vibration, corresponding to the polymeric shell of poly(styrene-divinylbenzene). In addition, peaks located between 1600 and 1500 cm<sup>-1</sup> confirmed the presence of C=C phenyl stretching [50–52]. In the spectrum of gypsum without NPCM, the band within at 3200 - 3800 cm<sup>-1</sup> denotes asymmetric stretching band of crystalline water. The band observed at 1150 cm<sup>-1</sup> represented the symmetric stretching vibration of O-H group in the water. Besides, the band recorded at 1619 cm<sup>-1</sup> was attributed to the bending vibration of S-O group in CaSO<sub>4</sub> [53,54]. The spectra of the composite gypsums with NPCM present the characteristic bands of the NPCM and the pure gypsum, demonstrating, undoubtedly, that the NPCMs are part of the gypsum matrix. Further, in Fig. 2, it can be observed that the characteristic bands from NPCM increase with its content in capsules.

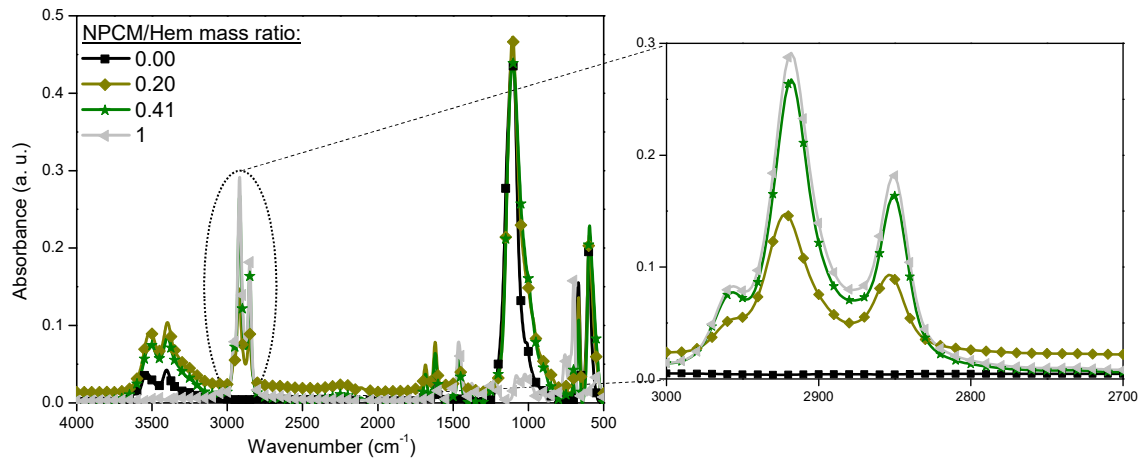


**Fig. 2.** FT-IR analyses of the gypsum composites C-NPCM/Hem<sub>0</sub>, C-NPCM/Hem<sub>0.2</sub> and C-NPCM/Hem<sub>0.41</sub> and the pure NPCM.

### Scanning Electron Microscopy (SEM) analysis

The presence of fillers can modify the morphology of calcium sulphate dihydrate crystal [47]. As an example, the structures of the composites C-NPCM/Hem<sub>0</sub>, C-NPCM/Hem<sub>0.2</sub>, C-NPCM/Hem<sub>0.3</sub> and C-NPCM/Hem<sub>0.41</sub> are shown in Fig. 3.



**Fig. 3.** SEM images of gypsums with different NPCM/Hem mass ratio.

According to Fig. 3, the crystal size of the gypsum increases with the presence of the NPCM; as an example, comparing the width of the biggest crystals found for C-NPCM/Hem<sub>0</sub> and C-NPCM/Hem<sub>0.41</sub>, they increased from 2.0 µm to 7.3 µm, respectively. Besides, the shape of the crystal is affected by them. The unmodified gypsum shows a needle-shape crystal structure (C-NPCM/Hem<sub>0</sub>). However, with the increase of NPCM tends to be hexagonal in shape. The use of slurries containing NPCMs and surfactants that are often crystal morphology modifiers to hydrate the hemihydrate, can affect the morphology in two ways; 1) the setting behavior with respect to time, and 2) the shape formation. Hence, according to the morphology, either PCM nanocapsules joined with the stabilizers promote Ostwald ripening during later stages of crystallization, or the agglomeration of nanoparticles takes place reducing the nucleation points during the setting stage. The nanocapsules agglomeration can be confirmed by SEM, since the areas indicated by white circles correspond to pores occupied by NPCMs. The location of the

lower density NPCM (dark areas) can be distinguished from the higher density gypsum crystals (bright areas) in the SEM images taken in backscattered mode.

### X-Ray Diffraction (XRD) analysis

Fig. 4.a shows the XRD analysis of the gypsums manufactured with different amounts of NPCM.

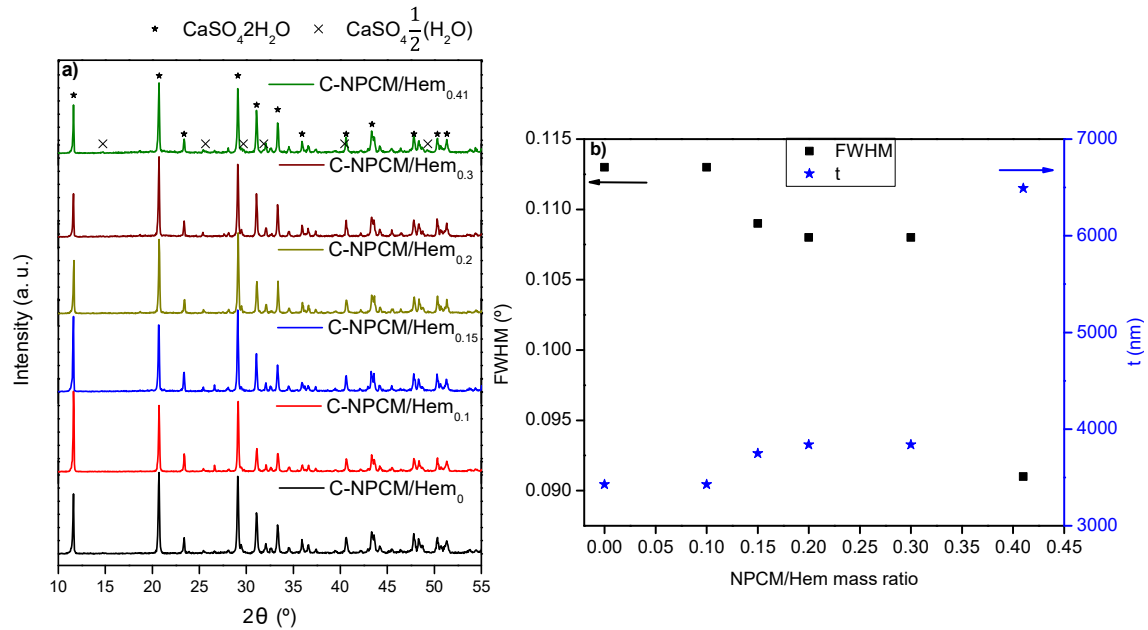


**Fig. 4.** a) X-Ray Diffraction patterns of the manufactured gypsums. b) Full width at half maximum (FWHM) and corresponding mean size of the crystallite ( $t$ ) obtained for the main peak located at  $2\theta = 11.6^\circ$  using the Debye-Scherrer formula for the gypsums prepared with different NPCM/Hem mass ratio.

In Fig. 4.a, it is observed that all the gypsums are mainly constituted by crystalline monoclinic calcium sulfate dihydrate ( $\text{CaSO}_4 \cdot 2\text{H}_2\text{O}$ ), with no important fingerprints from unreacted hemihydrate in XRD measurements, only revealing certain minor marks of unreacted orthorhombic hemihydrate ( $\text{CaSO}_4 \cdot \frac{1}{2}\text{H}_2\text{O}$ ), in the peaks located at  $2\theta = 25.4^\circ$ ,  $29.5^\circ$  and  $32.1^\circ$ . These vestiges of unreacted  $\text{CaSO}_4 \cdot \frac{1}{2}\text{H}_2\text{O}$  were a bit more pronounced for the reference gypsum without PCM (C-NPCM/Hem<sub>0</sub>) than for the gypsums including NPCM, exposing the dihydrate formation is slightly enhanced by the addition of NPCM. In contrast, all the gypsums showed very clear and narrow peaks related with monoclinic dihydrate ( $\text{CaSO}_4 \cdot 2\text{H}_2\text{O}$ ), principally located at  $2\theta = 11.6^\circ$ ,  $20.7^\circ$ ,  $23.4^\circ$ ,  $29.1^\circ$ ,  $31.1^\circ$ ,  $33.3^\circ$ ,  $35.9^\circ$ ,  $40.6^\circ$ ,  $43.5^\circ$ ,  $47.9^\circ$ ,  $50.3^\circ$  and  $51.3^\circ$ .

In Fig. 4.b, it is represented the decrease of FWHM as the NPCM/Hem ratio is augmented, revealing an increase of the crystallinity and domain size as the dose of NPCM is increased. From the reference gypsum (C-NPCM/Hem<sub>0</sub>) up to the gypsum C-NPCM/Hem<sub>0.3</sub>, the FWHM loss is moderate (from 0.113 to 0.108); however, for the gypsum containing the maximum amount of NPCM (C-NPCM/Hem<sub>0.41</sub>), such decline is more significant (FWHM = 0.091). In order to determine the mean size of the ordered crystalline domains in the manufactured gypsums, the Debye-Scherrer formula has been employed:

$$t = \frac{K \times \lambda}{\beta \times \cos\theta} \quad [3]$$

where  $t$  is the mean size of the crystallite,  $K$  is the Scherrer constant and taken equal to 0.9,  $\lambda$  is the wavelength of the Cu-K $\alpha$  radiation (1.54056 Å),  $\beta$  is the Full Width at Half Maximum (FWHM) of the X-ray peak in radians and  $\theta$  is the Bragg angle [55]. Thus, the mean size of the crystallite varies from 3427.0 up to 6491.8 nm, confirming the trend of crystallinity enhancement as the NPCM/Hem ratio is increased. Regarding  $t$ , the increase of crystallite size is modest between NPCM/Hem ratios 0.00-0.30, whereas a sudden and prominent augmentation is produced for the maximum dose of NPCM. These XRD findings are in good agreement with the evidence observed in SEM images, since the mean crystallite size increases as the NPCM amount is augmented, exactly the same behavior as the observed for the growth of the gypsums grains in SEM images when the NPCM/Hem ratio was raised.

### **Density and porosity**

Density (Fig. 5.a) and porosity (Fig. 5.b) of the manufactured gypsum composites are shown in Fig. 5.

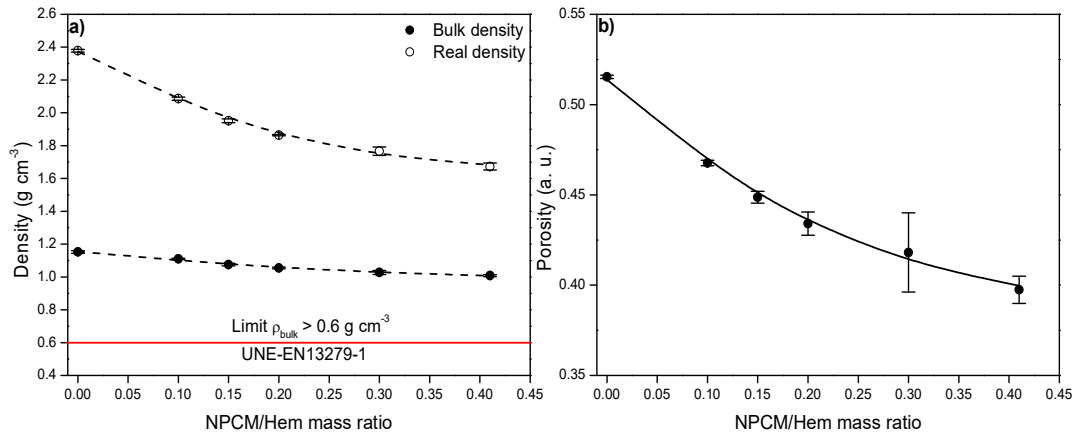


**Fig. 5.** a) Density and b) porosity of the composite gypsum blocks. Points were the mean of three specimens with whiskers representing the standard deviation interval.

As expected, the higher the NPCM content, the lower the composite bulk and real density (Fig. 5.a). This tendency can be explained attending to the lower density of the NPCM ( $0.96 \text{ g cm}^{-3}$ ) respect to that of the gypsum ( $2.38 \text{ g cm}^{-3}$ ). Although the bulk densities of the composites decrease with the NPCM content, all of them satisfy the minimum density value of  $0.60 \text{ g cm}^{-3}$  established by the European regulation UNE-EN 13279-1 for gypsum binders and gypsum plasters [56]. Fig. 5.b shows a decrease in the composite porosity with the NPCM content. In the SEM images (Fig. 3) can be confirmed that the presence of NPCMs modifies the shape structure of the gypsum crystals, but also their small size allows them to occupy the composite pores.

### Thermogravimetric analyses (TGAs) of gypsum composites

TGA of the gypsum composites with different NPCM/Hem mass ratios and the used NPCMs are shown in Fig. 6.

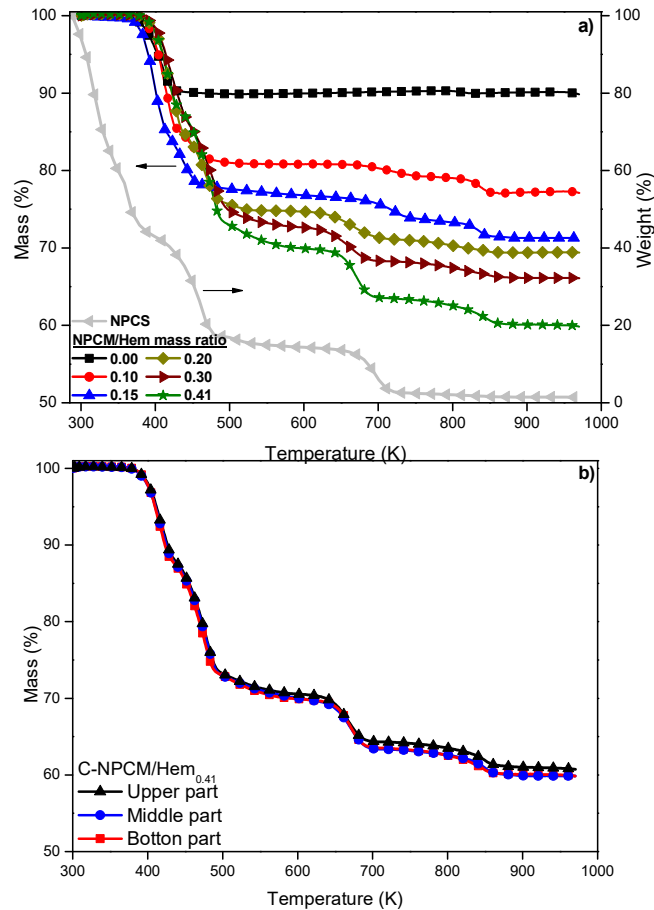


**Fig. 6.** a) Average of the TGA curves of the gypsum composites with different NPCM/Hem mass ratios and b) TGA curves of the different position of the same specimen with the higher NPCM/Hem mass ratio.

In Fig. 6.a, the TGA curve of the C-NPCM/Hem<sub>0</sub> presented three regions of mass loss. The first one, observed between 353 and 433 K, is attributed to absorbed water (hygroscopic water) and the chemically bound water of the hydrated salt. The second one, that occurs between 783 and 823 K, corresponds to the water bound to hydraulic compounds and the last one, the smallest one, refers to the CO<sub>2</sub> formed during the decomposition of carbonates [57,58]. The NPCS TGA curve presented four steps of mass loss. The first one, between room temperature and 393 K, is due to the water evaporation; the second one, between 413 and 483 K, corresponds to the RT27 evaporation; the third step, between 483 and 533 K, can be attributed to the surfactant degradation, and the last one, between 653 and 723 K is appropriate to the polymer degradation. Finally, a 1.5 % remains none degraded at 973 K due to the inorganic content of the surfactants. In the TGA curves of the gypsum composites can be observed four clear mass losses due to the absorbed water, the PCM, the polymer and the water bound to hydraulic compounds. The PCM and the polymer content present in each composite according to the TGA results is



shown in Table 3. It is worthy to point out that the biggest deviation, between the three TGA in the different points of the specimens, was only a 0.7 % in the case of PCM, for C-NPCM/Hem<sub>0.3</sub>. So, it is possible to say that the NPCMs have a good distribution in the composite when it is added in the form of NPCS, as it was confirmed by the TGA analyses of different points of the block from C-NPCM/Hem<sub>0.41</sub> (Fig. 6.b).

**Table 3.** Average and standard deviation of mass loss of the PCM and polymer in the gypsum composites with different NPCM/Hem mass ratios analyzed three times.

| Composites                 | PCM mass loss (%) | Polymer mass loss (%) |
|----------------------------|-------------------|-----------------------|
| C-NPCM/Hem <sub>0</sub>    | -                 | -                     |
| C-NPCM/Hem <sub>0.1</sub>  | 4.3 ± 0.3         | 1.8 ± 0.2             |
| C-NPCM/Hem <sub>0.15</sub> | 7.7 ± 0.1         | 2.8 ± 0.2             |
| C-NPCM/Hem <sub>0.2</sub>  | 9.3 ± 0.2         | 3.6 ± 0.1             |
| C-NPCM/Hem <sub>0.3</sub>  | 13.1 ± 0.7        | 4.9 ± 0.4             |
| C-NPCM/Hem <sub>0.41</sub> | 15.5 ± 0.1        | 6.4 ± 0.2             |

### Thermal behavior of the composite gypsum blocks

Fig. 7 shows the heat capacity of the synthesized composites using the NPCS as additive. The heat capacity has been calculated by DSC from two kind of experiments, one with a heating ramp and the other with cooling ramp.

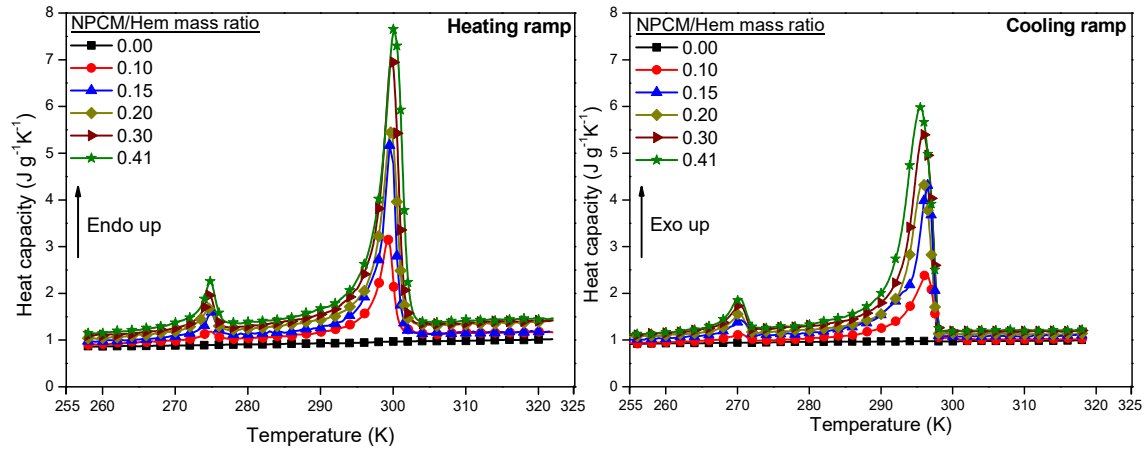


**Fig. 7.** Heat capacity versus temperature of the different composite gypsums measured by DSC.

As expected, the heat capacity ( $c_p$ ) of the gypsum blocks increases with the increase in the NPCM/Hem mass ratio (Fig. 7). It was calculated the average  $c_p$  (Table 4) in the PCM fusion interval (between 292 and 305 K) and the increase in the  $c_p$  with respect to the unmodified gypsum (C-NPCM-Hem<sub>0</sub>) was determined, with values of around 80, 140, 165, 208 and 269 %, for C-NPCM/Hem<sub>0.1</sub>, C-NPCM/Hem<sub>0.15</sub>, C-NPCM/Hem<sub>0.2</sub>, C-NPCM/Hem<sub>0.3</sub> and C-NPCM/Hem<sub>0.41</sub>, respectively. The latent heat of

each composite was calculated by integrating the  $c_p$  versus temperature curve in the paraffin melting temperature range, obtaining values of 0, 9.7, 16.5, 18.0, 25.7 and 30.2 J g<sup>-1</sup> for C-NPCM/Hem<sub>0</sub>, C-NPCM/Hem<sub>0.1</sub>, C-NPCM/Hem<sub>0.15</sub>, C-NPCM/Hem<sub>0.2</sub>, C-NPCM/Hem<sub>0.3</sub> and C-NPCM/Hem<sub>0.41</sub>, respectively. The latent heat relationship with the NPCM/Hem mass ratio was found to be linear, as can be observed in Fig. 8.

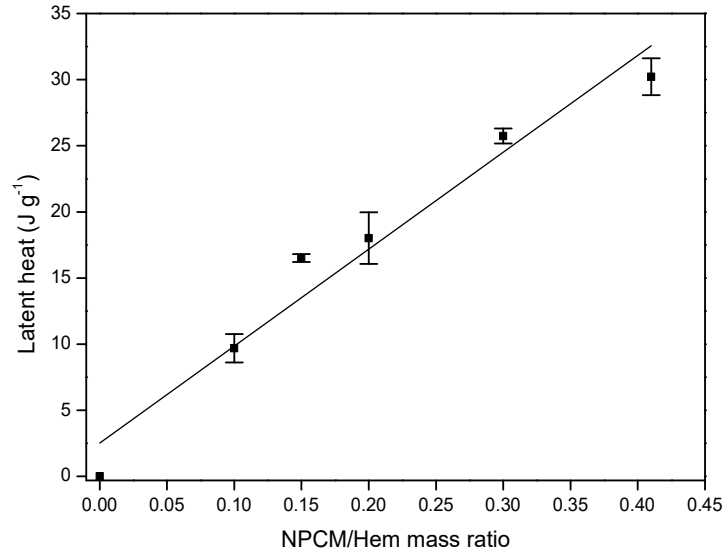


**Fig. 8.** Latent heat versus temperature of different composites measured by DSC. Points were the mean of three specimens with whiskers representing the standard deviation interval.

Fig. 9 shows the temperature profiles of the specimens containing NPCM when they were subjected to the heating process.

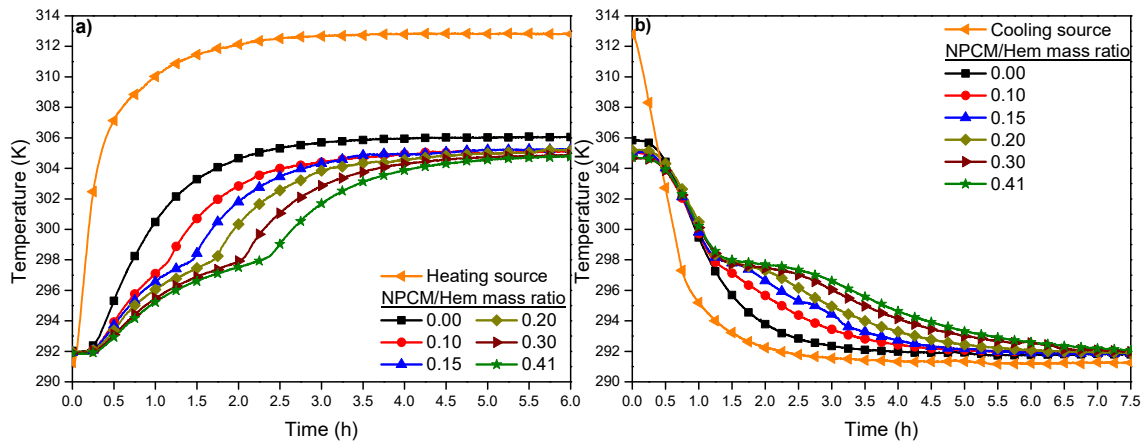


**Fig. 9.** Temperature profiles of the external surface of the composite blocks containing NPCM additive with the NPCM, a) Heating and b) Cooling

The results shown in Fig. 9 demonstrate that the higher the NPCM content in construction material, the lower the slope of the temperature profiles when the temperature reaches the region in which the PCM starts to melt or solidify (298 K). On

contrary to what happens for the case of gypsum without PCM, when PCM is present, an inflection point appears, since the thermal energy increases proportionally with respect to the amount of PCM present. This inflection point indicates that the PCM is absorbing the thermal energy leading its melting instead of increasing the gypsum block temperature (Fig. 9.a). The same happens when a temperature drop ramp is applied to the specimen (Fig. 9.b), but in this case the decrease in the temperature change is due to the fact that the PCM is releasing the thermal energy that was previously absorbed. In that way, the specimen C-NPCM/Hem<sub>0.41</sub> had the biggest buffering behavior allowing to delay in 2.36 h the heating steady state and in 3.89 h the cooling steady state. This was also confirmed by the increase of the absorbed and released with the addition of the NPCM, determined from the experimental equipment measurements (Fig. 10). Furthermore, it was observed a reduction of the temperature in the steady state for each composite respect to the pure gypsum, which could indicate a decrease of the thermal conductivity.

The difference between the heating or cooling sources respect to the temperature of upper surfaces is motivated by the thermal conductivity, the specimen thickness and the chamber temperature (298 K). The thermal conductivity and the thickness are practically the same, then the gap is mainly influenced by the difference between the steady state with the temperature of the environmental chamber. In that way, the narrower temperatures in the cooling process respect to the heating process is due to the gap between 291 K and 318 K respect to 298 K, respectively.

So, it can be also said that the insulating capacity of the composites has been improved, it could be explained attending to the low thermal conductivity of the NPCM which is within 0.1 - 0.2 W m<sup>-1</sup>K<sup>-1</sup>, which is lower than that of pure gypsum (0.2-0.8 W m<sup>-1</sup>K<sup>-1</sup>) [46,59–61].

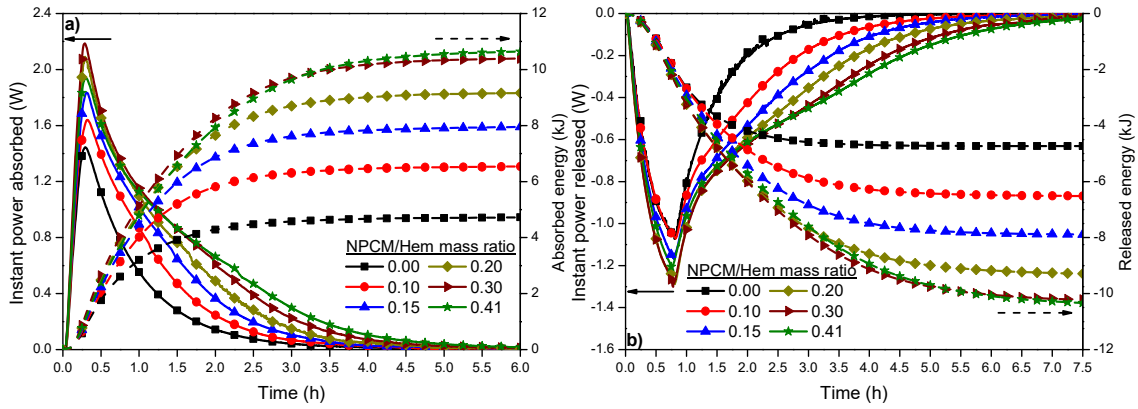


**Fig. 10.** Instant power and energy a) absorbed and b) released for the gypsum composites synthesized with the NPCM.

From the thermal analyses results, TES capacities per cubic meter in the range of the specimen temperature change were determined by using Eq. [2] (Table 4). These values increase with the increase of the NPCM content due to the latent heat of fusion of the PCMs and the polymer heat capacity. The TES capacities per cubic meter of the composite C-NPCM-Hem<sub>0.1</sub>, C-NPCM-Hem<sub>0.15</sub>, C-NPCM-Hem<sub>0.2</sub>, C-NPCM-Hem<sub>0.3</sub> and C-NPCM-Hem<sub>0.41</sub> increased by around 57, 89, 100, 133 and 140 %, respectively, compared with C-NPCM-Hem<sub>0</sub>. The TES capacity values are represented in Table 4. On the other hand, when temperature is below the melting point, the manufactured composite gypsums release all the thermal energy that they had absorbed. Hence, with these materials it is also possible to increase the accumulation of energy and also reduce the thermal loss because they have a thermal conductivity lower than the standard gypsum.

Fig. 11 presents the heat flux of the external surface of the specimens, which would correspond with the heat flow throughout the indoor surface of a wall, it means, the incoming or outgoing heat in a room. In that way, the negative heat flow values correspond to the heat transfer from the composite to the inside of a room.

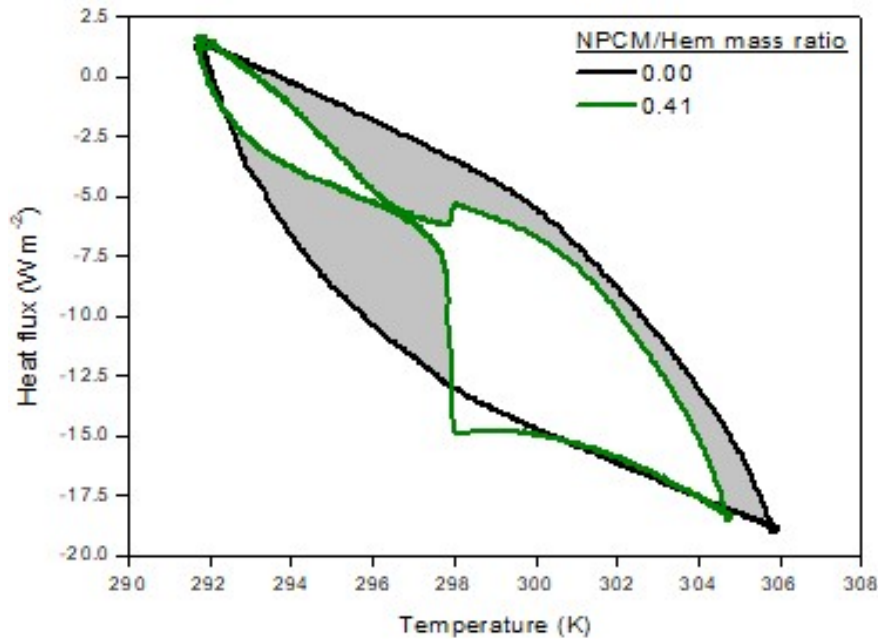


**Fig. 11.** Heat flux of the external surface of the composite blocks C-NPCM-Hem<sub>0</sub> and C-NPCM-Hem<sub>0.41</sub> for heating and cooling step.

It is plain to see that, in the heating step at the transient state the C-NPCM-Hem<sub>0</sub> exhibited a high incoming heat flux. On the contrary, the uptake of energy by the PCM in the composite (gray area) absorbed the incoming heat until temperature reached 298 K. Once that temperature was achieved, the greater portion of the composite had overpassed its melting temperature (Fig. 7), having no capacity to uptake more energy and increasing in that way the incoming heat flux into the room. Thus, the incorporation of NPCM greatly reduced the incoming heat from the outside during the transient states.

During the cooling step, when temperature was below 298 K, the heat flow reaches a plateau region that finishes at 296 K. This plateau area represents the solidification of the PCM, process in which the composite would transfer its previously stored heat to the room.

Finally, the thermal conductivity of all the manufactured specimens at different temperatures were measured by lambdometer (Fig. 12).

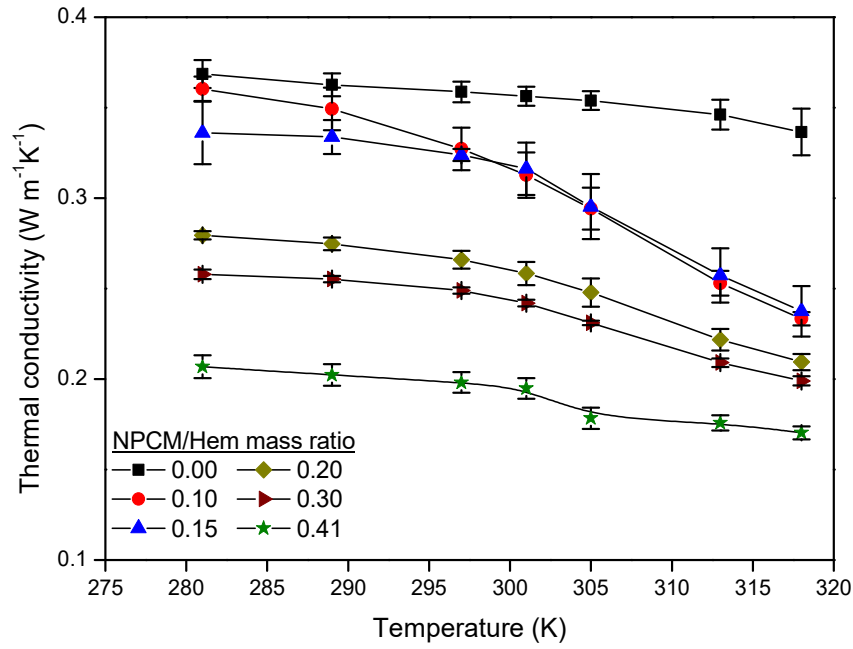


**Fig. 12.** Thermal conductivity the composite gypsum blocks at different temperatures determined by using a lambdometer. Points were the mean of three specimens with whiskers representing the standard deviation interval.

Fig. 12 shows the thermal conductivity ( $k$ ) decrease with the mass ratio of NPCM/Hem increase. The percentages of thermal conductivity reduction were around 17, 17, 30, 35 and 50 % at 305 K for C-NPCM-Hem<sub>0.1</sub>, C-NPCM-Hem<sub>0.15</sub>, C-NPCM-Hem<sub>0.2</sub>, C-NPCM-Hem<sub>0.3</sub> and C-NPCM-Hem<sub>0.41</sub>, respectively, compared with the pure gypsum (C-NPCM-Hem<sub>0</sub>). The measured  $k$  values at 305 K are gathered in Table 4. This reaffirms what was seen with the experimental setup (Fig. 9 and Fig. 10), where the maximum temperature reached in the steady state decreases when the mass ratio NPCM/Hem increased. Therefore, it can be concluded that the use of NPCM as additive to produce composite gypsums improves their insulating properties.

As a summary, Table 4 shows the thermal properties of the developer composites.

**Table 4.** Summary composite gypsums thermal properties. Represented the mean values of three replicated measurements together with the standard deviation.

| Composites                 | $k$ at 305 K<br>(W m <sup>-1</sup> K <sup>-1</sup> ) | $c_p$<br>(J g <sup>-1</sup> K <sup>-1</sup> ) | TES capacity<br>(kWh m <sup>-3</sup> ) |
|----------------------------|--|---|--|
| C-NPCM-Hem <sub>0</sub>    | 0.35 ± 0.01  | 1.0 ± 0.0                                     | 5.6 ± 0.1                              |
| C-NPCM-Hem <sub>0.1</sub>  | 0.29 ± 0.01  | 1.7 ± 0.1                                     | 8.8 ± 0.3                              |
| C-NPCM-Hem <sub>0.15</sub> | 0.30 ± 0.02  | 2.3 ± 0.0                                     | 10.6 ± 0.2                             |
| C-NPCM-Hem <sub>0.2</sub>  | 0.25 ± 0.01  | 2.5 ± 0.2                                     | 11.1 ± 0.2                             |
| C-NPCM-Hem <sub>0.3</sub>  | 0.23 ± 0.00  | 2.9 ± 0.2                                     | 13.0 ± 0.1                             |
| C-NPCM-Hem <sub>0.41</sub> | 0.18 ± 0.01  | 3.5 ± 0.2                                     | 13.5 ± 0.0                             |

Another important point related to the energy savings is the reduction of the CO<sub>2</sub> emissions to the atmosphere. The use of 1 m<sup>3</sup> of panels in the correct orientation of gypsum composites containing a 15 and 41 wt% of NPCM respect to the hemihydrate would allow to reduce 2.2 and 3.4 kg of CO<sub>2</sub> emissions per absorption/releasing operating cycle within 292 - 306 K, respectively. This is obtained considering that 0.42 kg of CO<sub>2</sub> are released to the atmosphere per one electric kWh of produced energy [62]. In Fig. 13, a DSC thermal cycling for the thermoregulating gypsums of maximum load is shown.

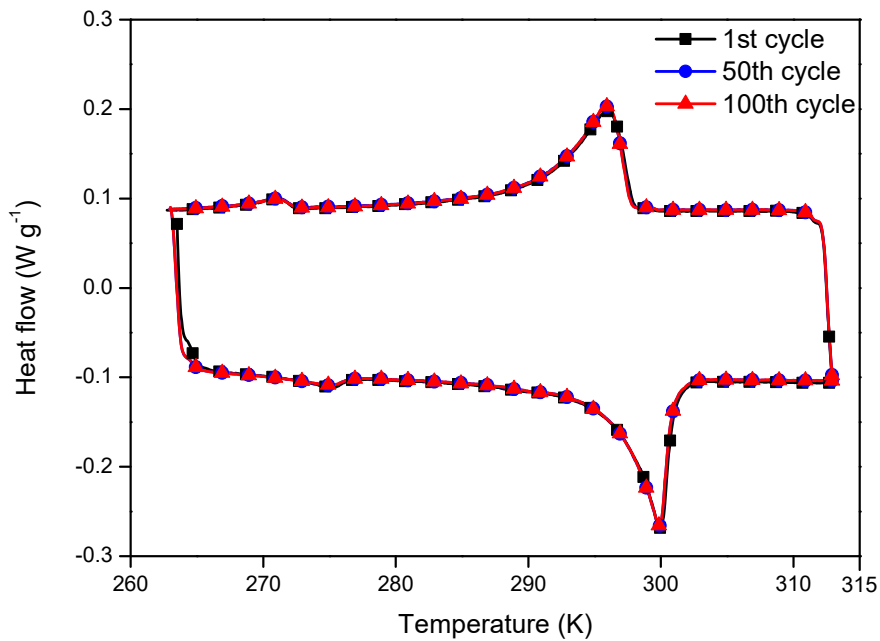


**Fig. 13.** Thermal heating/cooling cycling (263 to 313 K) for the C-NPCM/Hem<sub>0.41</sub> by DSC.

In Fig. 13 it can be perceived that the gypsum composite with maximum NPCM content revealed an excellent thermal cyclability, even after 100 heating/cooling cycles, so leading to a gypsum composite material that can resist storage-release cycles without losing its thermal energy storage capacity, neither presenting direct PCM leakage nor capsule breaking (which can also promote PCM losses) during this process. This large cyclability guarantee the long-term thermal stability of this kind of composites. Additionally, the endothermic and exothermic peaks are very close in temperature, indicating that gypsum reduces the nanocapsule subcooling.

### Mechanical tests

Once confirmed the improvement of the thermal properties of the gypsum by using the NPCM as additive, the mechanical properties of the synthesized composites were studied according to the European Standard UNE-EN 13279-2 [47].

Fig. 14 shows the variation of the maximum flexion and compression strengths of the gypsum composites, respectively, as function of the NPCM/Hem mass ratio and temperature, being they tested at room temperature (293 K), PCM melting point (300 K) and once the PCM is melted (318 K).

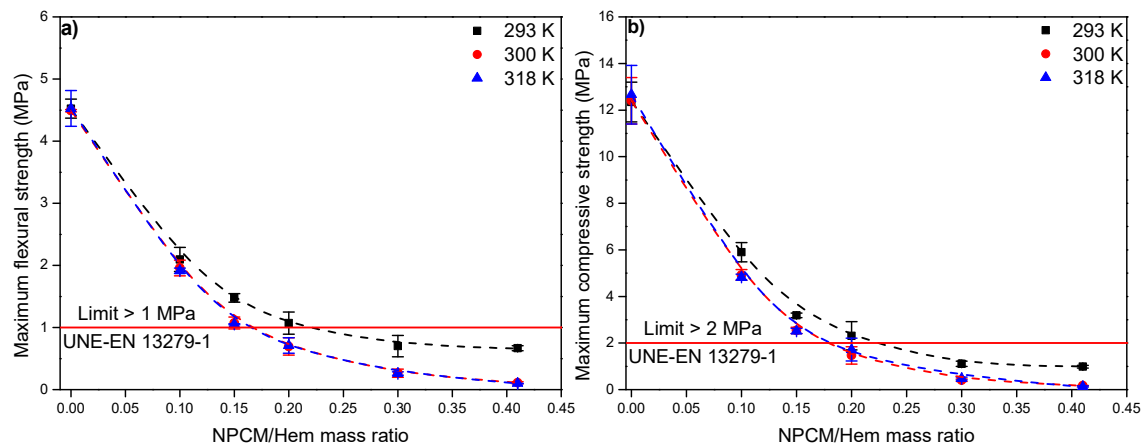


**Fig. 14.** Mechanical testing of the gypsum composites as function of mass ratio of NPCM/Hem, a) flexural strengths and b) compression strengths. Points were the mean of three specimens with whiskers representing the standard deviation interval.

The behavior of the maximum flexural and compressive strengths of the composites was quite similar, being possible to be explained in the same way. This is, the reduction in the mechanical strengths of the composites occurs either by temperature or NPCM content. The larger the NPCM/Hem mass ratio the lower the maximum flexion and compression strength of the composite. It is due to the reduction in density and the lower strength of the NPCM respect to the pure gypsum. The maximum flexural and compression strengths are higher for the composites tested at 293 K, when the PCM is solid, respect to the values obtained at 300 and 318 K, when the PCM is liquid. It could be explained attending to the PCM changes from solid to liquid, decreasing its strength and, therefore, its contribution to the strength of the composite. Besides, the mechanical strength decreases with the NPCM content. Taking into account the glass transition temperature of PS-DVB, which is higher than 95 °C, it does not contribute to the losing strength. Then, it is possible that the calcine of gypsum at 45 °C has a minimum contribution to this effect but it is more dependent on the melting temperature of the PCM



because it was not evidenced for the PCM-free gypsum. The maximum flexion and compression strengths reduction was observed for the composite C-NPCM-Hem<sub>0.41</sub>, reaching up to 85 and 87 %, respectively, when the tested temperature is shifted from 293 to 318 K. However, there is no significant variation between the measurements at 300 and 318 K, indicating that the composite thermal conductivity is high enough for ensuring that practically the total PCM melts at its melting point. Nevertheless, it is important to point out that the application of these composites is limited by mechanical strength, being only possible to consider these composites as gypsum binders or gypsum plasters those obtained from a NPCM/Hem mass ratio up to 0.15 which satisfy the European mechanical standard EN 13279-1 [56].

Considering the physical, thermal and mechanical properties of developed composites, some of these new materials can be used as construction gypsums for special applications, such as, gypsum plasterboard, drywall, plasterboard for ceilings and fiber-reinforced plasterboard [56].

## Conclusions

Smart gypsum composites were manufactured using a nanoencapsulated phase change material slurry containing nanocapsules from poly(styrene-co-divinylbenzene) as shell and paraffin wax as core materials. A uniform distribution of the nanocapsules in the composite was observed, being possible to use the slurry to hydrate the hemihydrate. A linear relationship between the latent heat of the gypsum composites and the nanocapsules content was verified. The heat capacity, the thermal energy storage capacity and thermal conductivity of the new building material were improved in 269, 140 and 50 %, respectively, when a 0.41 mass ratio of nanocapsules/hemihydrate was used. Composites from a nanocapsules/hemihydrate mass ratio up to 0.15 satisfied European mechanical standard EN 13279-1 for gypsum binders and gypsum plasters and all of them, presented a bulk density higher than 0.60 g cm<sup>-3</sup>. The presence of nanocapsules and surfactant changed the morphology of gypsum crystals during the setting stage. Thanks to the incorporation of such high amounts of nanocapsules, it is possible to reduce 3.4 kg of CO<sub>2</sub> emissions per operating cycle by using 1 m<sup>3</sup> of panels of this lightweight gypsum.

**Acknowledgements:** Authors gratefully acknowledge the financial support from the Spanish Ministry of Science, Innovation and Universities due to the project

TRANSENERGY (RTI2018-100745-B-I00) and the fellowship for PhD studies (FPU16/02345) of Daniel López Pedrajas.

## References

1. U.S. Energy Information Administration. International Energy Outlook 2020 [Internet]. 2021. Available from: <https://www.eia.gov/outlooks/ieo/>
2. Parlamento Europeo y Consejo de la Unión Europea. Directiva 2010/31/UE del Parlamento Europeo y del Consejo relativa a la eficiencia energética de los edificios. 2010.
3. Secretaría de Estado de Transportes M y AU. ERESEE 2020. Actualización 2020 de la estrategia a largo plazo para la rehabilitación energética en el sector de la edificación en España. 2020.
4. Podara CV, Kartsonakis IA, Charitidis CA. Towards phase change materials for thermal energy storage: classification, improvements and applications in the building sector. *Appl Sci*. 2021;11:1–26.
5. Leong KY, Abdul Rahman MR, Gurunathan BA. Nano-enhanced phase change materials: A review of thermo-physical properties, applications and challenges. *J Energy Storage*. 2019;21:18–31.
6. Jelle BP, Kalnæs SE. Phase Change Materials for Application in Energy-Efficient Buildings. *Cost-Effective Energy Effic. Build. Retrofit. Mater. Technol. Optim. Case Stud*. 2017.
7. Sarbu I, Sebarchievici C. A comprehensive review of thermal energy storage. *Sustain*. 2018;10:191.
8. Youssef Z, Delahaye A, Huang L, Trinquet F, Fournaison L, Pollerberg C, et al. State of the art on phase change material slurries. *Energy Convers Manag* [Internet]. Elsevier Ltd; 2013;65:120–32. Available from: <http://dx.doi.org/10.1016/j.enconman.2012.07.004>
9. Ghoghaei MS, Mahmoudian A, Mohammadi O, Shafii MB, Jafari Mosleh H, Zandieh M, et al. A review on the applications of micro-/nano-encapsulated phase change material slurry in heat transfer and thermal storage systems. *J Therm Anal Calorim* [Internet]. Springer International Publishing; 2021;145:245–68. Available from:

<https://doi.org/10.1007/s10973-020-09697-6>

10. Telkes M. Thermal energy storage in salt hydrates. *Sol Energy Mater.* 1980;2:381–93.
11. Serrano A, Borreguero AM, Garrido I, Rodríguez JF, Carmona M. Reducing heat loss through the building envelope by using polyurethane foams containing thermoregulating microcapsules. *Appl Therm Eng.* 2016;103:226–32.
12. Borreguero AM, Garrido I, Valverde JL, Rodríguez JF, Carmona M. Development of smart gypsum composites by incorporating thermoregulating microcapsules. *Energy Build.* 2014;76:631–9.
13. Hawes DW, Banu D, Feldman D. Latent heat storage in concrete. II. *Sol Energy Mater.* 1990;21:61–80.
14. Sarier N, Onder E. Thermal characteristics of polyurethane foams incorporated with phase change materials. *Thermochim Acta.* 2007;454:90–8.
15. Sánchez L, Sánchez P, de Lucas A, Carmona M, Rodríguez JF. Microencapsulation of PCMs with a polystyrene shell. *Colloid Polym Sci [Internet].* 2007;285:1377–85. Available from: <https://www.scopus.com/inward/record.uri?eid=2-s2.0-36649033608&doi=10.1007%2Fs00396-007-1696-7&partnerID=40&md5=aceec06fb8a65b24084382f6a7627295>
16. Borreguero AM, Carmona M, Sanchez ML, Valverde JL, Rodriguez JF. Improvement of the thermal behaviour of gypsum blocks by the incorporation of microcapsules containing PCMS obtained by suspension polymerization with an optimal core/coating mass ratio. *Appl Therm Eng.* 2010;30:1164–9.
17. Kahraman Doğüşcü D, Kızıl Ç, Biçer A, Sarı A, Alkan C. Microencapsulated n-alkane eutectics in polystyrene for solar thermal applications. *Sol Energy.* 2018;160.
18. Sami S, Sadrameli SM, Etesami N. Thermal properties optimization of microencapsulated a renewable and non-toxic phase change material with a polystyrene shell for thermal energy storage systems. *Appl Therm Eng.* 2018;130.
19. Borreguero AM, Valverde JL, Rodríguez JF, Barber AH, Cubillo JJ, Carmona M. Synthesis and characterization of microcapsules containing Rubitherm®RT27 obtained by spray drying. *Chem Eng J.* 2011;166:384–90.

20. Mohammadi B, Najafi FS, Ranjbar H, Mohammadi J, Zakaryazadeh M. Nanoencapsulation of butyl palmitate in polystyrene-co-methyl methacrylate shell for thermal energy storage application. *Energy Build* [Internet]. Elsevier; 2016 [cited 2020 Mar 12];118:99–105. Available from: <https://www.sciencedirect.com/science/article/pii/S0378778816300913?via%3Dihub>
21. Maleki B, Khadang A, Maddah H, Alizadeh M, Kazemian A, Ali HM. Development and thermal performance of nanoencapsulated PCM/ plaster wallboard for thermal energy storage in buildings. *J Build Eng*. 2020;32:101727.
22. Khadiran T, Hussein MZ, Syamsi HW, Zainal Z, Rusli R. Laboratory-scale studies on smart gypsum composite boards incorporated with nano-encapsulated organic phase change material for thermal comfort building application. *J Mater Civ Eng*. 2016;28:04015137.
23. Mert MS, Mert HH, Yilmaz Gumus C. Preparation and characterization of paraffin microcapsules for energy-saving applications. *J Appl Polym Sci*. 2019;136.
24. Stejskalová K, Bujdoš D, Procházka L, Smetana B, Zlá S, Teslík J. Mechanical, Thermal, and Fire Properties of Composite Materials Based on Gypsum and PCM. *Materials (Basel)*. 2022;15:1253.
25. Lachheb M, Younsi Z, Naji H, Karkri M, Ben Nasrallah S. Thermal behavior of a hybrid PCM/plaster: A numerical and experimental investigation. *Appl Therm Eng*. 2017;111.
26. Serrano S, Barreneche C, Navarro A, Haurie L, Fernandez AI, Cabeza LF. Use of multi-layered PCM gypsums to improve fire response. Physical, thermal and mechanical characterization. *Energy Build*. 2016;127.
27. Srinivasaraonaik B, Singh LP, Sinha S, Tyagi I, Rawat A. Studies on the mechanical properties and thermal behavior of microencapsulated eutectic mixture in gypsum composite board for thermal regulation in the buildings. *J Build Eng*. 2020;31:101400.
28. de la Paz Miguel M, Vallo CI. Influence of the emulsifying system to obtain linseed oil-filled microcapsules with a robust poly (melamine-formaldehyde)-based shell. *Prog Org Coatings*. 2019;129.

29. He Y, Yao S, Hao J, Wang H, Zhu L, Si T, et al. Synthesis of melamine-formaldehyde microcapsules containing oil-based fragrances via intermediate polyacrylate bridging layers. *Chinese J Chem Eng.* 2019;27.
30. Pan X, York D, Preece JA, Zhang Z. Size and strength distributions of melamine-formaldehyde microcapsules prepared by membrane emulsification. *Powder Technol.* 2012;227.
31. Cao VD, Pilehvar S, Salas-Bringas C, Szczotok AM, Valentini L, Carmona M, et al. Influence of microcapsule size and shell polarity on thermal and mechanical properties of thermoregulating geopolymer concrete for passive building applications. *Energy Convers Manag.* 2018;164.
32. Borreguero AM, Rodríguez JF, Valverde JL, Peijs T, Carmona M. Characterization of rigid polyurethane foams containing microencapsulated phase change materials: Microcapsules type effect. *J Appl Polym Sci.* 2013;128.
33. Chen X, Kong X, Wang S, Fu X, Yu B, Yao K, et al. Microencapsulated phase change materials: Facile preparation and application in building energy conservation. *J Energy Storage.* 2022;48:104025.
34. Peng G, Dou G, Hu Y, Sun Y, Chen Z. Phase change material (PCM) microcapsules for thermal energy storage. *Adv Polym Technol.* 2020;2020:9490873.
35. Peng H, Wang J, Zhang X, Ma J, Shen T, Li S, et al. A review on synthesis, characterization and application of nanoencapsulated phase change materials for thermal energy storage systems. *Appl Therm Eng* [Internet]. Elsevier Ltd; 2021;185:116326. Available from: <https://doi.org/10.1016/j.applthermaleng.2020.116326>
36. ISO. International Standard ISO/TS 80004-1. Nanotechnologies - Vocabulary - Part 1: Core terms. 2015;
37. Sukhorukov G, Fery A, Möhwald H. Intelligent micro- and nanocapsules. *Prog Polym Sci.* 2005;30:885–97.
38. Xu B, Li P, Chan C. Application of phase change materials for thermal energy storage in concentrated solar thermal power plants: A review to recent developments. *Appl Energy.* 2015;160:286–307.
39. Liu H, Wang X, Wu D, Ji S. Fabrication and applications of dual-responsive

microencapsulated phase change material with enhanced solar energy-storage and solar photocatalytic effectiveness. *Sol Energy Mater Sol Cells*. 2019;193:184–97.

40. Zhang Y, Wang K, Tao W, Li D. Preparation of microencapsulated phase change materials used graphene oxide to improve thermal stability and its incorporation in gypsum materials. *Constr Build Mater* [Internet]. Elsevier Ltd; 2019;224:48–56. Available from: <https://doi.org/10.1016/j.conbuildmat.2019.06.227>

41. Zhang Y, Tao W, Wang K, Li D. Analysis of thermal properties of gypsum materials incorporated with microencapsulated phase change materials based on silica. *Renew Energy* [Internet]. Elsevier Ltd; 2020;149:400–8. Available from: <https://doi.org/10.1016/j.renene.2019.12.051>

42. Carmona Franco M, Rodríguez Romero JF, Borreguero Simón AM, Garrido Sáenz I, Ramos Mellado FJ, López-Pedrajas D, et al. Procedimiento de obtención in situ de fluidos térmicos que contienen partículas termorreguladoras sub-micrónicas [Internet]. España; 2021. Available from: <https://consultas2.oepm.es/InvenesWeb/detalle?referencia=P201930715>

43. OFICEMEN. Standard UNE-EN 196-1. Methods of testing cement. Part 1: Determination of strength. 2018;1–40.

44. Borreguero AM, Luz Sánchez M, Valverde JL, Carmona M, Rodríguez JF. Thermal testing and numerical simulation of gypsum wallboards incorporated with different PCMs content. *Appl Energy*. Elsevier Ltd; 2011;88:930–7.

45. Barreneche C, De Gracia A, Serrano S, Elena Navarro M, Borreguero AM, Inés Fernández A, et al. Comparison of three different devices available in Spain to test thermal properties of building materials including phase change materials. *Appl Energy*. 2013;109:544–52.

46. Borreguero AM, Serrano A, Garrido I, Rodríguez JF, Carmona M. Polymeric-SiO<sub>2</sub>-PCMs for improving the thermal properties of gypsum applied in energy efficient buildings. *Energy Convers Manag*. 2014;87:138–44.

47. AENOR. Standard UNE-EN 13279-2. Gypsum binders and gypsum plasters. Par2: Test methods. 2014;

48. Kim D, Jung J, Kim Y, Lee M, Seo J, Khan SB. Structure and thermal

properties of octadecane/expanded graphite composites as shape-stabilized phase change materials. *Int J Heat Mass Transf.* 2016;95:735–41.

49. Mekaddem N, Ali SB, Fois M, Hannachi A. Paraffin/expanded perlite/plaster as thermal energy storage composite. *Energy Procedia.* 2019. p. 1118–29.

50. Barholin M, Boissier G, Dubois J. Styrene-divinylbenzene copolymers, 3. Revisited IR analysis. *Die Makromol Chemie.* 1981;7:2875–2085.

51. Szczotok AM, Carmona M, Kjøniksen A-L, Rodriguez JF. The role of radical polymerization in the production of thermoregulating microcapsules or polymers from saturated and unsaturated fatty acids. *J Appl Polym Sci.* 2018;135:45970.

52. Salgado-Pizarro R, Padilla JA, Xuriguera E, Barreneche C, Fernández AI. Novel shape-stabilized phase change material with cascade character: Synthesis, performance and shaping evaluation. *Energies.* 2021;14:2621.

53. Knittle E, Phillips W, Williams Q. An infrared and Raman spectroscopic study of gypsum at high pressures. *Phys Chem Miner.* 2001;28:630–40.

54. Karaipekli A, Sarı A, Biçer A. Thermal regulating performance of gypsum/(C18–C24) composite phase change material (CPCM) for building energy storage applications. *Appl Therm Eng.* 2016;107:55–62.

55. Patterson AL. The scherrer formula for X-ray particle size determination. *Phys Rev.* 1939;56:978–82.

56. AENOR. Standard UNE-EN 13279-1. Gypsum binders and gypsum plasters. Part 1: Definitions and requirements. 2009;

57. Greco A, Maffezzoli A, Manni O. Development of polymeric foams from recycled polyethylene and recycled gypsum. *Polym Degrad Stab.* 2005;90:256–63.

58. Anastasiou M, Hasapis T, Zorba T, Pavlidou E, Chrissafis K, Paraskevopoulos KM. TG-DTA and FTIR analyses of plasters from byzantine monuments in Balkan region : Comparative study. *J Therm Anal Calorim.* 2006;84:27–32.

59. Feldman D, Banu D, Hawes D, Ghanbari E. Obtaining an energy storing building material by direct incorporation of an organic phase change material in gypsum wallboard. *Sol Energy Mater.* 1991;22:231–42.

60. Chen C, Guo H, Liu Y, Yue H, Wang C. A new kind of phase change material (PCM) for energy-storing wallboard. *Energy Build.* 2008;40:882–90.

61. Toppi T, Mazarella L. Gypsum based composite materials with micro-encapsulated PCM: Experimental correlations for thermal properties estimation on the basis of the composition. *Energy Build.* 2013;57:227–36.

62. U.S. Energy Information Administration. How much carbon dioxide is produced per kilowatthour of U.S. electricity generation? [Internet]. 2020. Available from: <https://www.eia.gov/tools/faqs/faq.php?id=74&t=11>